Geophys. J. Int. (2005) **163,** 852–862 doi: 10.1111/j.1365-246X.2005.02777.x

Analytical and 3-D numerical modelling of Mt. Etna (Italy) volcano inflation

A. Bonaccorso,[1] S. Cianetti,[2] C. Giunchi,[2] E. Trasatti,[2] M. Bonafede[3] and E. Boschi[3]

[1] *Istituto Nazionale di Geofisica e Vulcanologia, Sezione di Catania, Italy*
[2] *Istituto Nazionale di Geofisica e Vulcanologia, Sismologia e Tettonofisica, Roma, Italy. E-mail: giunchi@ingv.it*
[3] *Università degli Studi di Bologna, Dipartimento di Fisica, Settore Geofisica, Bologna, Italy*

Accepted 2005 August 4. Received 2005 March 31; in original form 2004 October 6

SUMMARY

Since 1993, geodetic data obtained by different techniques (GPS, EDM, SAR, levelling) have detected a consistent inflation of the Mt. Etna volcano. The inflation, culminating with the 1998–2001 strong explosive activity from summit craters and recent 2001 and 2002 flank eruptions, is interpreted in terms of magma ascent and refilling of the volcanic plumbing system and reservoirs. We have modelled the 1993–1997 EDM and GPS data by 3-D pressurized sources to infer the position and dimension of the magma reservoir. We have performed analytical inversions of the observed deformation using both spheroidal and ellipsoidal sources embedded in a homogeneous elastic half-space and by applying different inversion methods. Solutions for these types of sources show evidence of a vertically elongated magma reservoir located 6 km beneath the summit craters. The maximum elevation of topography is comparable to such depth and strong heterogeneities are inferred from seismic tomography; in order to assess their importance, further 3-D numerical models, employing source parameters extracted from analytical models, have been developed using the finite-element technique. The deformation predicted by all the models considered shows a general agreement with the 1993–1997 data, suggesting the primary role of a pressure source, while the complexities of the medium play a minor role under elastic conditions. However, major discrepancies between data and models are located in the SE sector, suggesting that sliding along potential detachment surfaces may contribute to amplify deformation during the inflation. For the first time realistic features of Mt. Etna are studied by a 3-D numerical model characterized by the topography and lateral variations of elastic structure, providing a framework for a deeper insight into the relationships between internal sources and tectonic structures.

Key words: finite-element methods, geodesy, lateral heterogeneity, volcanic activity, volcanic structure.

1 INTRODUCTION

Mt. Etna volcano is located on the eastern margin of Sicily, one of the most tectonically active areas of the world. Rising 3320 m above sea level and extending for 40 km in basal diameter, Mt. Etna is the biggest active volcano in Europe and one of the best monitored in the world. The continuous development of monitoring systems and the frequent eruptions in the last decades have improved the knowledge of the volcano during its different phases of activity. However, an intriguing question is still open and concerns the existence of a magma chamber beneath the volcano, which may be responsible for deformation of the entire edifice. To date, seismic tomography studies have failed to show evidence of any large magma chamber within the uppermost 10 km (see Chiarabba *et al.* 2004, for an overview).

Instead, storage zones smaller than the resolving power of seismic tomography could well exist in this part of the upper crust, as suggested by petrological data, which indicate that this depth range can be considered as a neutral buoyancy level where magma can stagnate being surrounded by rocks with the same density (Corsaro & Pompilio 2004). However, the most spectacular evidence of magmatic storage activity comes from geodetic observations revealing movements of the entire edifice that may be consistent with a pressure source located 3–5 km below sea level. One of the best examples is the overall inflation during the 1980s, interrupted by several small deflations associated with minor eruptions, culminating with the main overall deflation during the 1991–1993 eruption (see Bonaccorso & Davis 2004, for references). This is the most significant effusive event in the last three centuries, which produced $\sim 235 \times 10^6$ m^3 of lava in 476 days, leaving, in the geodetic records, a strong deflation signal, associated with mass depletion and loss of internal pressure (Bonaccorso 1996). Another independent evidence of deflation comes from interferometric images by

satellite synthetic aperture radar (SAR) (Massonnet *et al.* 1995; Lanari *et al.* 1998). After the 1991–1993 eruption, the volcano started a new phase of continuous and marked inflation. The ground deformation, measured by electro-optical distant measurements (EDM) and global positioning system (GPS) showed an areal expansion (Puglisi *et al.* 2001; Bonaccorso & Davis 2004), which almost uniformly increased from the end of the 1991–1993 eruption to 2001, indicating, together with the seismic activity, an overall continuous accumulation of tension inside the volcano (Patanè *et al.* 2003). The recharging period was ended by a shallow small dike emplacement at the beginning of 1998 (Bonaccorso & Patanè 2001), followed by the summit eruptions with lava pouring out from craters in 1999 February–November and 2001 January–May, and by several tens of spectacular lava fountains from the summit craters during 1998–2001 (La Delfa *et al.* 2001; Alparone *et al.* 2003; Behncke & Neri 2003). All these phenomena suggested a progressive magma upraising that heralded the 2001 July–August and the 2002 October flank eruptions.

Therefore, the 1993–1997 time interval may be considered as an almost pure recharge phase due to the over-pressurization of a shallow depth reservoir causing a net inflation of the volcano. The aim of the paper is to study the 1993–1997 deformations and the characteristics of the associated source by using analytical and numerical models. The comparison between analytical models in a simple homogeneous medium and more advanced numerical models is focused on examining the effects caused by the topography and the subsurface heterogeneities.

In the following section we provide more details on the 1993–1997 inflation phase. In Section 3, we describe results obtained by analytical models to retrieve position and shape of the pressure source. These results are used for the calibration and application of the FE numerical model as described in Section 4. Finally, we discuss the parameters inferred according to the different models for the shape and location of the pressure source, together with the limitations of the present approach and implications for future research.

2 1993–1997 INFLATION PHASE

As revealed by EDM, GPS, levelling and tilt measurements, the 1991 December to 1993 March eruption was characterized by very low seismicity and continuous deflation. After the end of the eruption, seismic activity resumed and an extraordinary inflation phase started. During 1994–1996, significant magma uprising was detected by positive microgravity anomalies, interpreted as the accumulation of new magma at 3 km below sea level (Budetta *et al.* 1999). After the first increasing phase, the gravity anomalies decreased from 1997 to 1999, suggesting a source located S–SE of the summit craters, at 3–4 km depth below sea level (Carbone *et al.* 2003). The decreasing gravity during 1997–1999 could be associated either with gas exsolution and expansion or with the decrease in solubility of the volatile component. Both effects result in a net density decrease (Carbone *et al.* 2003). The beginning of the inflation pattern was also confirmed by SAR images collected during the first 2 yr of the recharging period (1993–1995). From the inversion of the interferograms, a spheroidal magmatic source located beneath the summit at 5 km below sea level was retrieved (Lundgren *et al.* 2003).

The developing of the recharging phase was better detected by the geodetic measurements. The vertical displacements recorded from 1994 to 1998 by high-precision levelling showed significant uplift of several centimetres. Obrizzo *et al.* (2004), performing a Bayesian inversion of these vertical data, suggest a simple point source model (Mogi 1958) most likely located N of the central craters at 4.5 km below sea level. The inflation process was also clearly evident in the yearly geodetic measurements recorded by EDM and GPS networks managed by INGV (Fig. 1a). These data (Fig. 1b) showed a near uniform expansion of each sector monitored by EDM and of the overall volcano edifice (GPS). Usually, the line length variations may be helpful to evaluate the uniform strain tensor ϵ_{ij}, which is a concise representation of the strain field (Jaeger 1969). A convenient representation is given by the time evolution of the cumulative areal

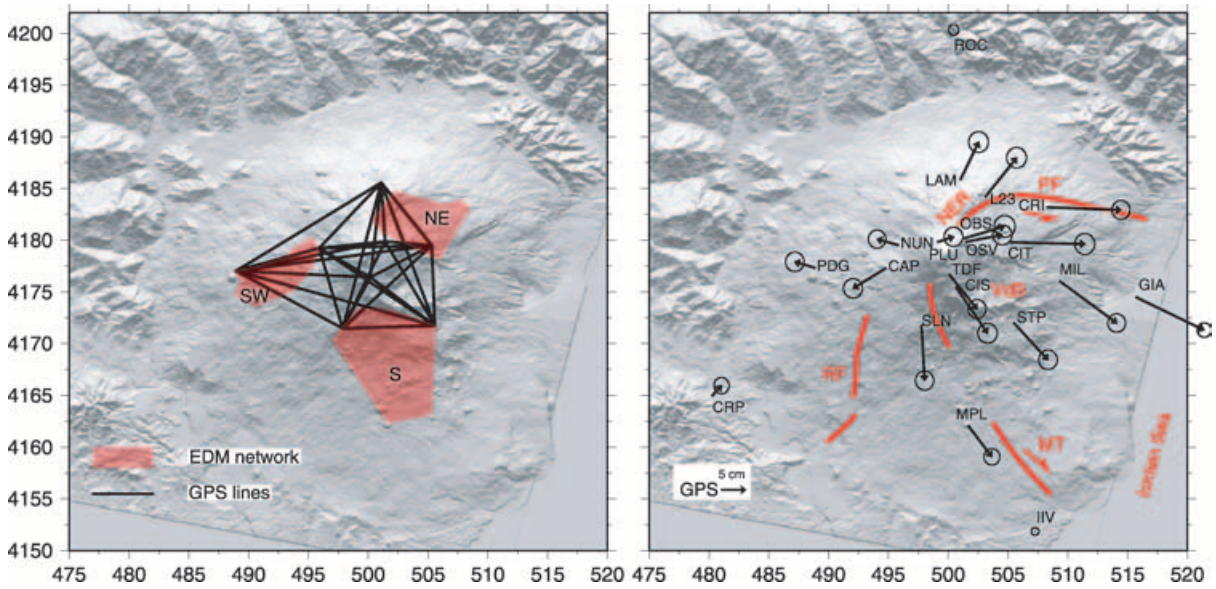

Figure 1. Left, Mt. Etna geodetic networks. The red patches show areas covered by the three sections of the EDM network. The black lines show the GPS baselines. Right, GPS horizontal displacements recorded at Mt. Etna from 1993–1997. For each GPS station, name and ellipse error is also shown. The red lines show the major surface fault systems bordering the eastern and southern sectors of the volcano (NER = north east rift, PF = Pernicana fault, MT = Mascalucia–Trecastagni fault; RF = Ragalna fault; VdB = Valle del Bove). Geographical coordinates are expressed in UTM projection.

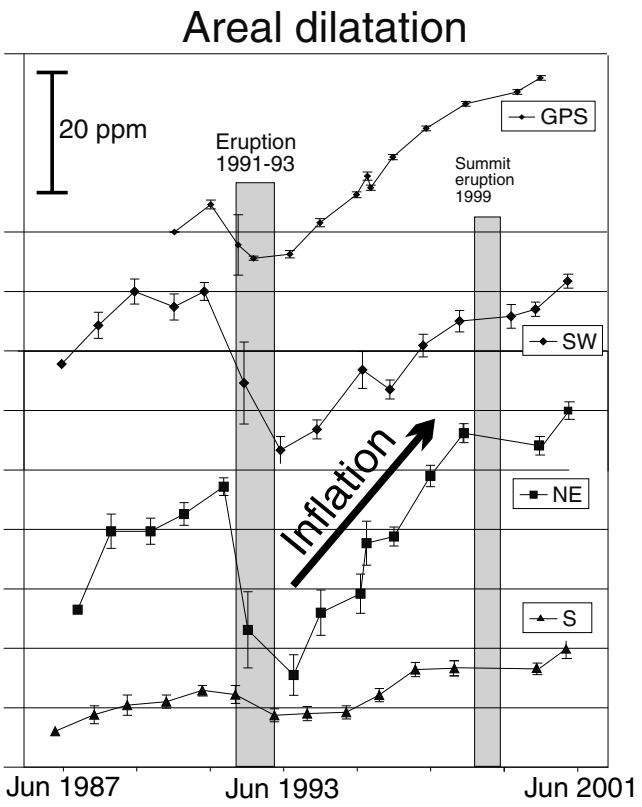

Figure 2. Cumulative planar areal dilatation of Mt. Etna in the last 15 yr, computed for the networks shown in Fig. 1. A fairly continuous expansion affected the volcanic edifice starting from 1993 to the 2001 flank eruption.

dilatation $D = \epsilon_{11} + \epsilon_{22}$, which shows that all the monitored sectors have undergone a nearly constant areal expansion rate (Fig. 2).

The radial pattern shown by the horizontal displacements computed from 1993–1997 GPS measurements clearly reveal the inflation phase (Fig. 1b). However, a seaward sliding seems to affect the SE flank, where displacement vectors do not decay in amplitude on moving away from the summit area towards the Ionian Sea. Furthermore, some of these stations undergo a negative vertical displacement (MIL and GIA). This evidence has been interpreted as an eastwards sliding associated with a gravitational instability (e.g. Borgia *et al.* 1992; Lo Giudice & Rasà 1996; Rust & Neri 1996). Despite being affected by this flank instability, the 1993–1997 period represents a very interesting phase of increasing pressurization of the plumbing system that was not perturbed by eruptive activity, which resumed in 1998 from the summit caters and was followed by the 2001 July–August and 2002 October to 2003 January flank eruptions (Patanè *et al.* 2003).

3 ANALYTICAL MODELLING OF ETNA DEFORMATION

Our purpose in this section is to model the EDM and GPS deformation data by analytical solutions based on a single source in a homogeneous half-space, trying to determine its position and geometry. Although the data may be not representative of a pure inflation, it is nonetheless worth understanding to what extent a single source is able to fit observed deformations.

The data set is composed of 147 EDM and GPS baseline changes and of 20 GPS vertical displacements recorded in the 1993–1997 span. The GPS and EDM networks are located on the volcano edifice at an average elevation of 1700 m above sea level (Fig. 1a). This height will be considered in the following analytical models as the reference surface, neglecting the topography of Mt. Etna.

Two analytical models of pressurized sources are used. These models are implemented within two distinct inversion methods, which allow us to constrain the geometrical and mechanical source properties, giving insights into the internal volcanic structure. The two analytical models have some common features: both are embedded in an elastic homogeneous Poissonian half-space ($\nu = 0.25$, i.e. $\lambda = \mu$). However, due to the simple elastic rheology, both models are affected by a trade-off between source volume V, internal overpressure ΔP and medium rigidity μ, since the analytical expressions of displacements contain a factor $\Delta PV/\mu$.

3.1 DAVIS inversion

The first inversion, DAVIS, is performed using the model by Davis (1986), a point pressurized cavity of ellipsoidal shape, arbitrarily oriented in the half-space (Fig. 3). The equations are implemented in a non-linear least-square inversion algorithm (Marquardt 1963), which allows retrieving nine parameters: three centre coordinates (SX, SY, SZ) and six independent P_{ij} components of the symmetrical stress tensor, with their associated uncertainties. The eigenvectors of the stress tensor provide the ellipsoid axes direction cosines, while the eigenvalues are related to the c/a and the b/a ratios of the ellipsoid axes (Davis 1986).

The inversion results indicate a source located a few hundred metres SE of the summit craters at a depth of ∼4 km below sea level (SX = 500.700 ± 0.3 km, SY = 4177.964 ± 0.3 km, in UTM reference frame; SZ = 4.200 ± 0.3 km b.s.l.). The eigenvalue analysis of P_{ij} matrix obtained from the inversion indicates a source with a vertically elongated shape. The semi-major axis a is almost three times b and c, which have comparable lengths. The angles $\phi = 124^\circ$ and $\delta = 77^\circ$ (indicating the orientation of the surface projection with respect to east direction and the dip of the ellipsoid major axis, respectively) show that the ellipsoid dips toward NW, almost vertically. The stress tensor P_{ij} is determined by the least-square inversion, which provides an estimated error of about 10 to 15 per cent. P_{ij} is linked to the geometrical parameters of the ellipsoidal source by complex analytical relationships involving elliptical

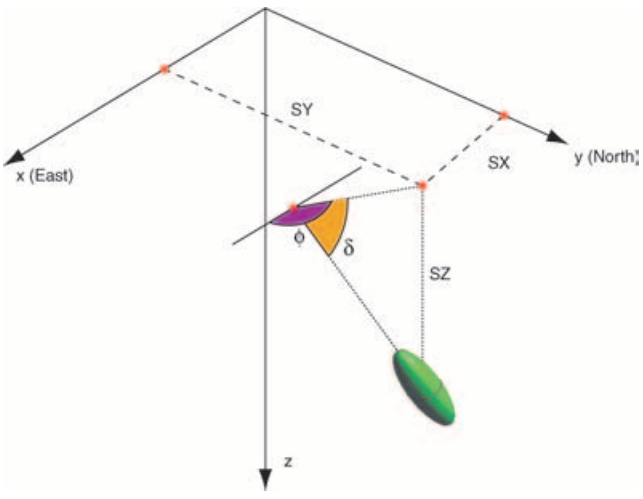

Figure 3. Model geometry for the ellipsoidal/spheroidal source used in the analytical inversion.

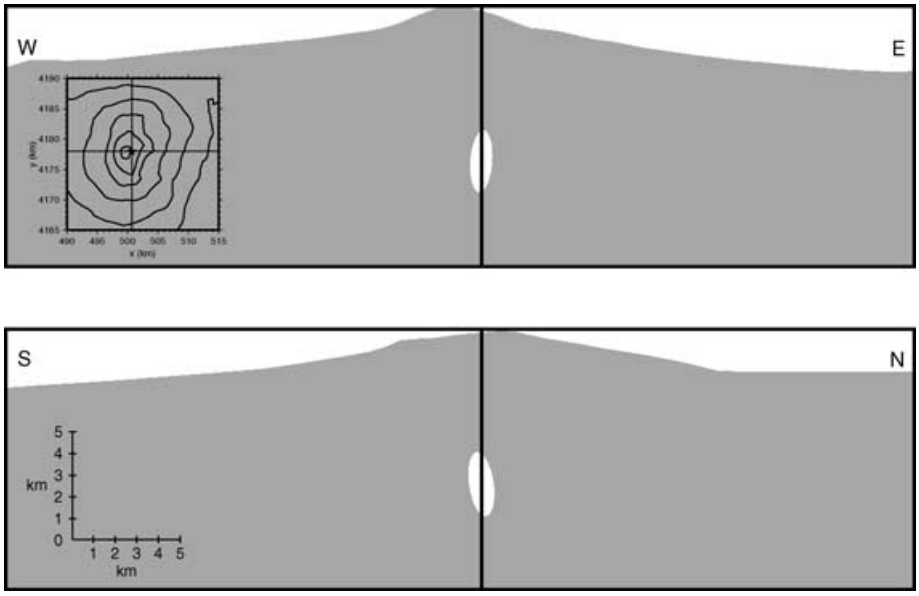

Figure 4. The inverted source geometry imaged by two vertical cross-sections intersecting at its centre. Top, WE section; bottom, SN section.

integrals (Davis 1986), therefore, it is not possible to evaluate directly the errors on the parameters a, b and c. However, we have verified, by a Monte Carlo analysis, that these parameters are affected by the same indetermination characterizing the P_{ij} coefficient (i.e. 10–15 per cent).

While the position and orientation of the source are directly determined by the inversion procedure, the source volume computation is possible only by fixing some parameter values since the P_{ij} components contains the factor $\Delta PV/\mu$. For the internal hydrostatic overpressure we obtain $\Delta P = 60 \times 10^6\, \mu/V$ (SI units). If we consider an effective shear modulus $\mu = 10^9$ Pa and a pressure increase $\Delta P = 20 \times 10^6$ Pa this implies a source volume of 3×10^9 m^3 with a semi-major axis of ∼1854 m and the other two axes of 725 and 544 m, respectively. A sketch of the cavity under these conditions is shown in Fig. 4. The retrieved source volume is reasonable since it is of the same order as the resolving power of the seismic tomography studies, which failed to show a evidence for a large reservoir.

3.2 YANG inversion

The second inversion procedure is based on simulated annealing, a global optimization algorithm (Mosegaard & Tarantola 1995). This method consists of an optimized search in the parameter space without *a priori* constraints. The search is very exhaustive since it is not limited to a downhill descent to minimize the chosen misfit function, but allows going uphill according to a certain probability. This probability decreases as a function of the number of accepted models, thus avoiding being trapped by local minima. The advantages of this technique are also accompanied by drawbacks, such as a slow convergence rate, the difficult tuning of the parameters inversions and the loss of mathematical accuracy, characteristic of non-probabilistic approaches (e.g. Press *et al.* 1997). The forward model used with the simulated annealing, YANG, is the finite spheroidal source developed by Yang *et al.* (1988).

The analytical implementation of the equations is much simpler than the DAVIS source and much less computationally demanding. This issue is very important since, for each inversion, the evaluation of several tens of thousand models is required. In this case the seven inverted parameters for the finite spheroid model are (Fig. 3): the source position SX, SY, SZ, the spheroid semi-axes a and b and their direction cosines ϕ and δ. The last parameter, ΔP, is fixed at 20 MPa as in the previous inversion.

The significance of the best-fitting model parameters (SX = 500.152 km, SY = 4178.694 km in UTM reference; SZ = 4.847 km b.s.l.; $a = 3396$ m, $b = c = 466$ m; $\phi = 94^\circ$, $\delta = 85^\circ$) can be better appreciated by examining Fig. 5, where the frequencies of statistically equivalent models at 95 per cent confidence level (selected by an F-test) are plotted. These histograms show how the parameter space is sampled by models with an equivalent capability to reproduce deformation data. This means that the width of the histograms can be considered as a measure of the errors of the inverted parameters: narrow histograms correspond to best-constrained parameters. Figs 5(a), (b) and (c) show that the source location is well constrained at a few hundred metres NW of the DAVIS source, and at a slightly higher depth. Also the dip angle $\delta > 85^\circ$ (Fig. 5e) is well determined by the inversion, thus confirming the previous finding. Also in this case we found a vertically elongated source with semi-major axis a not well constrained but greater than 2000 m, while the most likely value for b is ∼400 m. The volume of the pressurized source is 3.1×10^9 m^3, in agreement with the DAVIS inversion. Fig. 5(d) shows that 90° is the preferred value for the spheroid orientation ϕ.

3.3 Analytical inversions results

The comparison between observed and predicted data for the best fitting DAVIS and YANG models are shown in Fig. 6. The horizontal displacement for the GPS stations considered in the inversion is portrayed in Fig. 6(a). The overall pattern of computed horizontal deformation resembles the radial pattern of measured displacements, especially considering that we are dealing with a single pressurized source in an elastic homogeneous half-space, a crude assumption for volcanic areas. The vertical displacements predicted by the proposed models (Fig. 6b) always overestimate the observations but the computed trend matches the data. Both DAVIS and YANG models, however, fail to predict the negative vertical displacement recorded at MIL and GIA, which could be caused by the subsidence associated with a flank eastward sliding. The EDM elongations of 147 lines (20 of which linking GPS stations) are pretty well reproduced

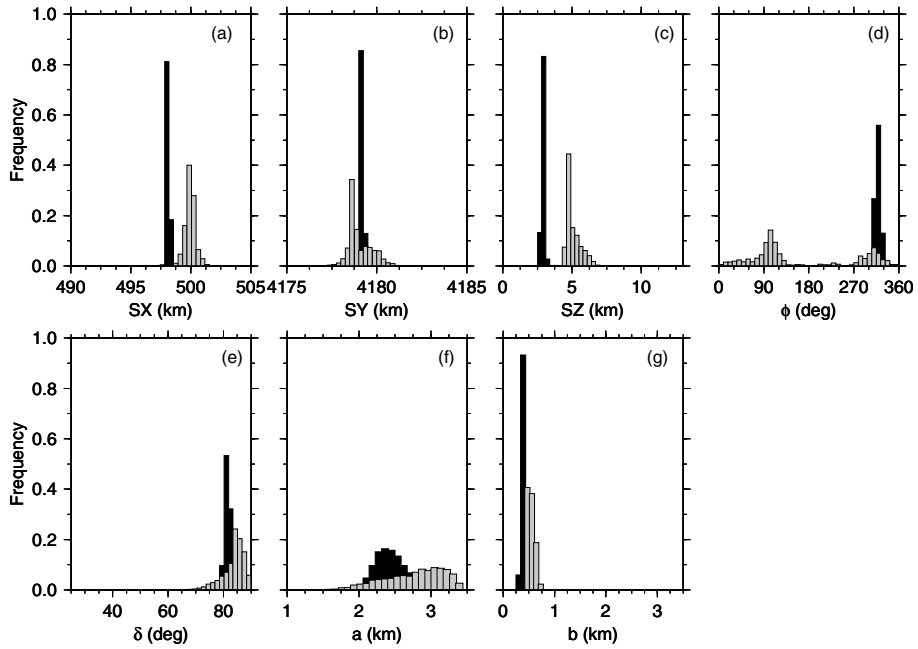

Figure 5. Simulated annealing inversion of the full data set (grey histograms) and of the partial data set (black histograms) consisting of GPS stations not located the lower SE sector: SX and SY are source position in UTM reference, SZ depth b.s.l., a, b spheroid semi-axes, ϕ semi-major axis angle with respect to east direction, δ semi-major axis dip. The histograms show the frequency of a subset of models in the parameters space, giving an indication of the sensitivity of the inversion procedure to each searched parameter. The selected models are characterized by a statistical equivalence in fitting the data.

by the best fitting models (Fig. 6c). The results of both models are similar but slightly better for the DAVIS model, which is characterized by nine parameters instead of 8. The residuals in Fig. 7 support this conclusion.

In the last few years the role of the E flank sliding has been debated by many authors. Several studies put forward geological and structural evidence for a sliding of the eastern and southern sectors of the volcano toward E and S, respectively (e.g. Borgia *et al.* 1992; Lo Giudice & Rasà 1996; Rust & Neri 1996; Bonforte & Puglisi 2003). The eastern sector, moving faster, is bounded in the northern part by the North Rift zone and by the E–W trending left lateral-transtensive Pernicana fault; the southern sector is delimited by the Mascalucia–Trecastagni fault systems (Fig. 1b). Some authors (e.g. Rust & Neri 1996; Neri *et al.* 2004) consider the southern sector to be widening in the western part up to reaching the Ragalna fault system. Recently, SAR interferometric images, recorded from 1993 to 1998, suggested a spreading associated with S–SE flank instability (Froger *et al.* 2001). The deformation in the eastern flank is interpreted as driven mainly by regional extensional dynamics, while the deformation of the southern sector as driven mainly by gravity spreading.

In summary, the current deformation of the volcano may result from the expansion of the whole edifice superimposed on a secondary, but relevant, sliding movement of the southern and eastern sectors as shown by Fig. 7. It is noteworthy to underline that in our single source modelling, the analytic inversion tries to fit the eastern displacements, obviously without full success, either increasing the factor $\Delta PV/\mu$ or deepening the source. As a consequence, both YANG and DAVIS best-fitting models overestimate displacement in the W sector of Mt. Etna, while they severely underestimate deformation of the E and SE sectors. This effect must be accounted for to explain the residual pattern in the W and SE sectors. While the eastward trend of the residuals in the SE sector may be due to the above mentioned flank instability, the same trend in the W sector, for which no evidence of instability has been shown, may be exclusively related to the inadequacy of the forward model to reproduce the deformation of the two flanks at the same time.

A further inversion was then performed employing the YANG model with GPS data from stable stations only (i.e. removing stations CRI, GIA, MIL, CIT, STP and MPL in the lower SE sector). The results are displayed in Fig. 5 as black histograms. The best fitting source is again a vertically elongated ellipsoid ($a = 2100$ m, $b =$ 325 m, $\delta = 82^\circ$, $\phi = 330^\circ$) with its centre at a slightly lower depth (SZ = 2.927 km b.s.l.) but shifted ~2 km to W (SX = 498.200 km, SY = 4179.200 km). The confidence intervals for the previous source parameters are much narrower than those obtained when using the full data set (see Fig. 5), but this can be largely attributed to the fact that the data set is severely reduced. It appears then that the 'anomalous' displacements in the SE sector may bias at least some of the source parameters. In any case, the vertically elongated shape of the source seems to be a very robust inference. However, it must be noted that the flank instability with eastward sliding is not the only possible explanation for the significant horizontal displacements of the low-altitude GPS stations in the E–SE sector. Different interpretations might be proposed for the asymmetric deformation, since the topography of Mt. Etna is rather asymmetric with a prominent mass deficit in the E sector with respect to the W sector, in correspondence of Valle del Bove. Moreover, the buried elastic structure inferred from recent seismic tomography studies also shows the presence of a high rigidity body centred below the SE sector. In the next section we shall investigate how the topography and the elastic heterogeneities may affect the computed deformation in a fully 3-D model.

4 FE MODELLING

In previous sections we showed that inversion procedures based on simple analytical models can be useful to infer source

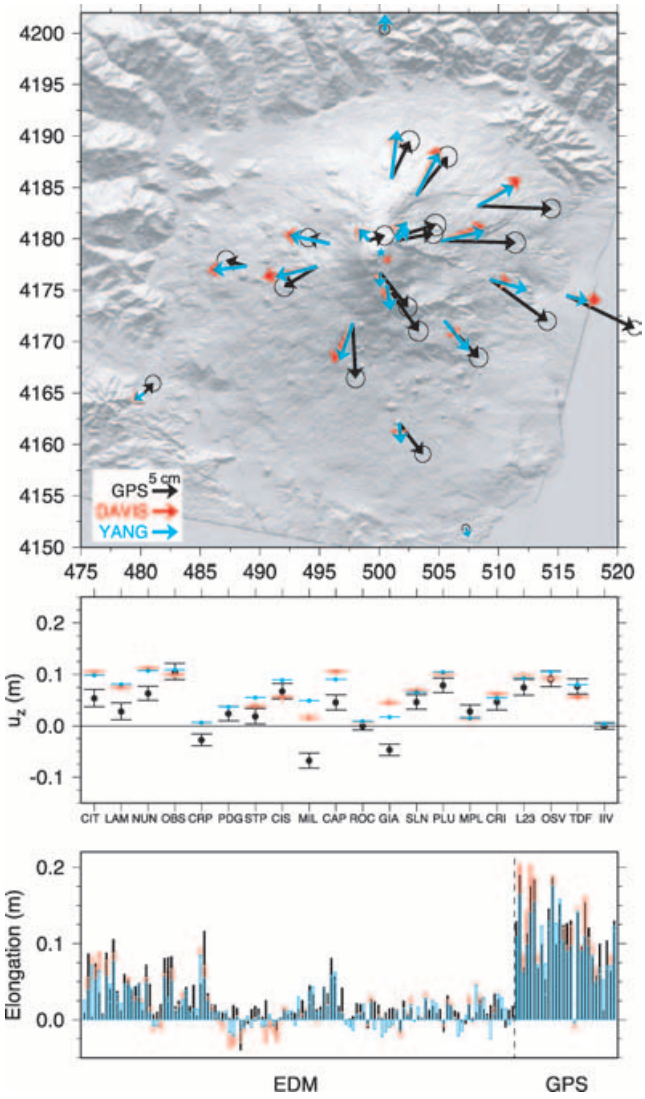

Figure 6. Comparison between predicted (DAVIS and YANG models, see text) and observed (GPS and EDM) deformation data. (a) GPS horizontal displacements (the stars are the projections onto the surface of source centres); (b) vertical displacements and (c) EDM (left) and GPS (right) elongations.

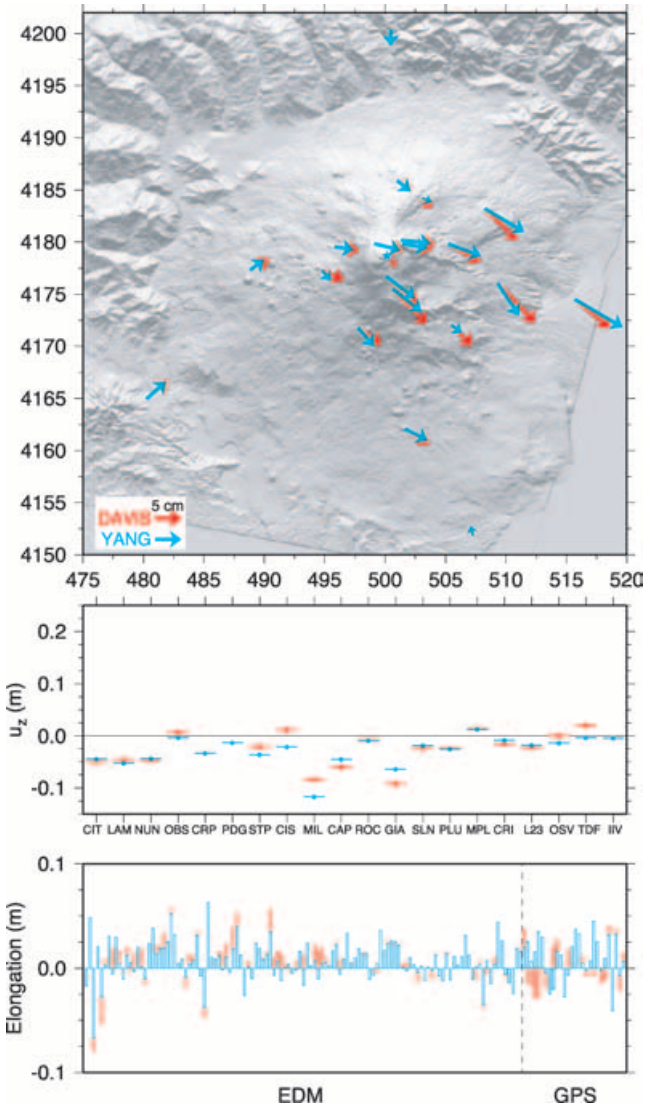

Figure 7. Residuals between modelled and observed data. (a) horizontal displacements; (b) vertical displacements and (c) EDM and GPS elongations.

parameters under strongly simplified assumptions. However, in volcanic areas more advanced modelling may be appropriate. Features like steep topographic relief, complex shape of the magmatic reservoir, elastic heterogeneities, anisotropy and rheological properties of the medium may affect the deformation pattern and can be investigated by the finite-element (FE) technique. In this study we focus our attention on the role played by two factors corresponding to the best-constrained features: Mt. Etna topography and the layering of elastic rigidity as derived from tomographic investigation. Topography is likely to be important since the inferred source depth b.s.l. in the previous models is comparable to the summit elevation a.s.l.. Furthermore, Bonafede & Rivalta (1999) have shown that stress (and deformation) is strongly affected by the presence of elastic heterogeneities when a tensile crack crosses the interface between different layers.

The FE domain (Fig. 8) extends 150 × 150 × 60 km^3 and is composed of 44 288 eight-nodes, isoparametric, arbitrarily distorted brick elements. The mesh resolution is about 100 m around the source, about 750 m at the surface above the source and progressively decreases to 10 km in the far field. The assumed boundary conditions are: fixed bottom displacements and fixed cavity overpressure $\Delta P =$ 20 MPa. First the FE grid is benchmarked by a comparison with analytical models. This test is done for both YANG and DAVIS sources over a 100 × 100 km^2 area centred above the cavity origin for two different source depths and different source orientations (results are not shown). The choice of the benchmark parameters was made taking into account the analytical inversion results. The analytical and numerical techniques well agree for all the YANG–type sources, validating the FE approach. For DAVIS–type sources, a small difference was instead found in a very small area above the source, being more evident for the case $\delta = 60°$. This difference can be attributed to the point-source approximation employed by DAVIS, while an extended source is considered in the FE model; the same discrepancy was already noted by Yang *et al.* (1988) (see their Figs 5a and b for $a/z_0 = 0.4$).

The good results attained with the benchmark encourage us to implement models where topography and rigidity layering are included. We would like to remind the reader that we are not implementing FE forward models inside an inversion procedure to

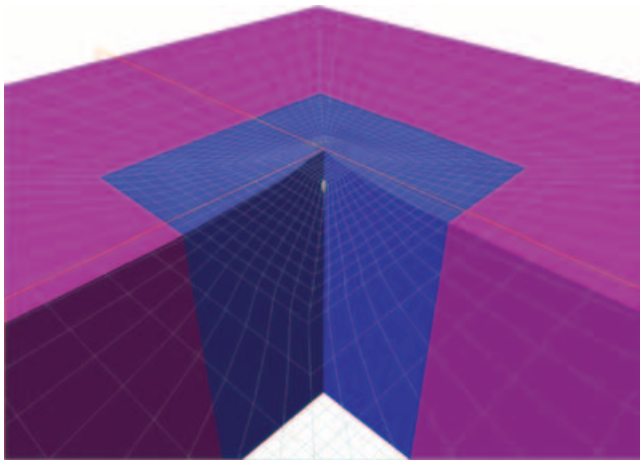

Figure 8. Picture of the FE model domain, viewed from SE. The blue section has an extension of about 50 × 50 km and is characterized by the Mt. Etna topography with increased resolution. The whole models measure about 150 × 150 × 60 km to minimize the effects of the imposed boundary conditions. The SE section of the model is removed so that the ellipsoidal source is visible. The grey lines show the surface mesh.

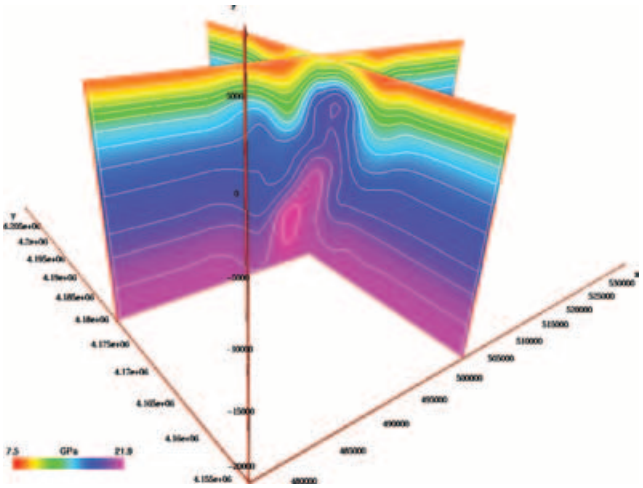

Figure 9. Heterogeneous rigidity distribution used in FE modelling computed from the tomographic results by Chiarabba *et al.* (2000). The SE view in UTM coordinates show very clearly the high rigidity body underneath Mt. Etna. The two cross-sections are centered on the summit craters.

find the optimized parameters as we did for the analytical models: we use the source parameters inferred from the analytical models within a more realistic description of the medium. Accordingly, the predictions of the new models are likely to be worse than the old ones, since the optimization is not performed. However, our aim is to evaluate the effects of neglecting the complexities associated with morphology and rheology of Mt. Etna in standard analytical studies.

A good strategy to understand how each single factor affects the forward prediction is to include each one in separate models and compare the results. For the following computations, the FE models share the same source location, geometry, and material properties (for homogeneous cases) of DAVIS. Since analytical inversions retrieve very similar source parameters for both DAVIS and YANG dilatation centres, we do not consider FE models for YANG source. We perform a first calculation by including Mt. Etna Topography in a HOmogeneous elastic structure model (hereinafter model HOT). Then we show the effects of elastic heterogeneities by a model with HEterogeneous rheology but Flat free surface (HEF) and, finally, a last model in which both features are combined (HET) in order to obtain a heterogeneous medium with real topography.

Mt. Etna topography in HOT and HET computation is introduced in a restricted 50 × 50 km^2 area centred on the Summit craters, and is extended, beyond this boundary, to a flat surface (Fig. 8). In models HEF and HET, rheological heterogeneities are computed converting the seismic velocity v_p by Chiarabba *et al.* (2000) to shear modulus using a reference density of 2500 kg m^{-3}. Two E–W and N–S cross-sections of the Mt. Etna elastic structure deduced from seismic tomography are shown in Fig. 9, evidencing a high rigidity volume located SE with respect to the summit craters, dipping slightly NW. This 3-D elastic structure was included in the numerical model by assigning to each element the value of shear modulus interpolated at the correct location. The values for the shear modulus obtained in this way (7.5–21.9 GPa) are, on average, more than 10 times larger than their homogeneous counterparts (1 GPa), which can be considered as the effective low rigidities usually employed in analytical modelling of volcanic areas. The discrepancy between seismic shear modulus μ_s and effective shear modulus μ_e is a well-known problem in volcanic deformation modelling.

The 'effective rigidity' concept is useful to justify that volcanic deformation models can be driven by not exceedingly high overpressures. This concept is physically motivated by the fact that the assumed elastic rheology may not be appropriated in proximity of the source where the medium behaviour may be better described as viscoelastic (at relatively high temperature) or at low confining pressure where the medium could have a plastic behaviour (Davis *et al.* 1974). Several rheological laws might be employed to model these inelastic effects, but they are usually based on the assumption that the deviatoric stress relaxes or even vanishes in the long-term. Accordingly, if the inelastic effects are restricted in a small volume around the source, the overpressure, applied to the interior surface of the cavity, will spread toward the outer boundary of the anelastic domain. A very simple example of such a mechanism was described by Dragoni & Magnanensi (1989) and applied to model the deformation field at Long Valley Caldera (Newmann *et al.* 2001). According to this model, the long-term deformation of the medium, away from the source, is proportional to $\Delta PV'/\mu$ where V' is the volume of the plastic region surrounding the reservoir. The deformation attained using an effective volume $V' = 10\,V$ would also be modelled by using an effective rigidity $\mu' = \mu/10$ or an effective pressure $P' = 10\,P$. In the following, we will assume that the medium is indeed elastic, with rigidity values equal to the short-term ones, inferred from seismic wave tomography. In order to reproduce the observed amplitudes of displacements, an effective pressure of ∼320 MPa is needed, which can be interpreted as 20 MPa of magma pressure (the same value inferred from the previous analytical inversions) in a small reservoir surrounded by a plastic volume 16 times greater.

Fig. 10 shows the horizontal, vertical and elongations data and their uncertainties (black) together with results attained with models HOT (green), HEF (pink) and HET (blue). The FE models predictions are very similar to the DAVIS source. This finding was already achieved by previous investigations (e.g. Trasatti *et al.* 2003), but it is confirmed here in a fully 3-D model. Effects due to topography are mostly evident only in the summit area: horizontal and vertical displacements predicted at PLU, OSV, OBS, CIS and TDF stations are sensibly different for model HET and HOT with respect to HEF or DAVIS (Fig. 11) characterized by a flat surface. Neither shear modulus heterogeneities nor topography may be responsible for the high displacements towards SE recorded by geodetic stations in the

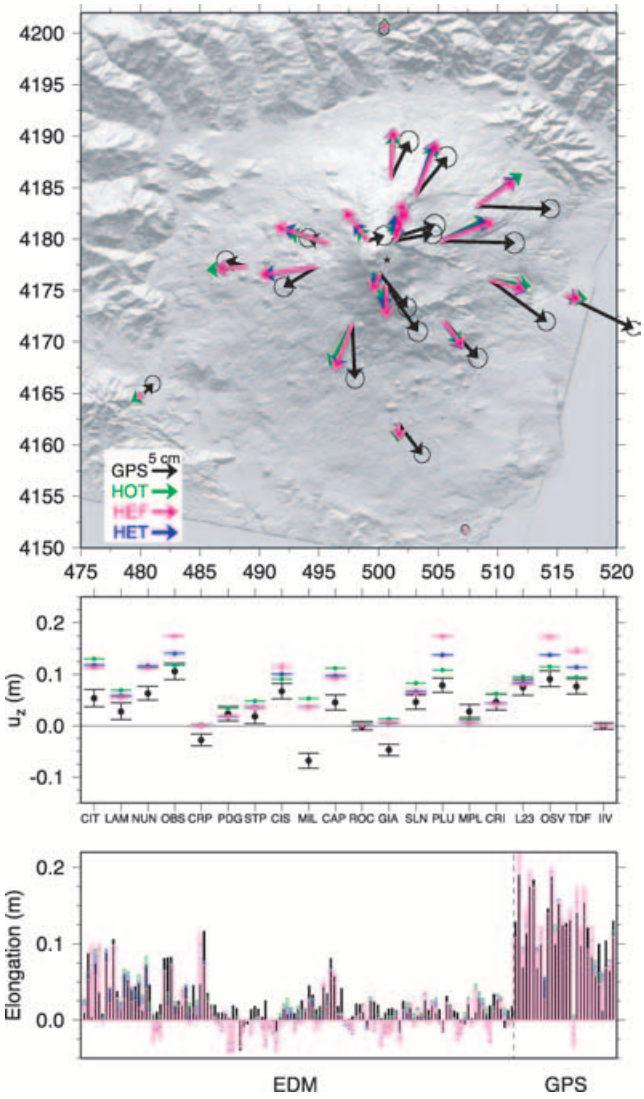

Figure 10. Comparison between observed data and FE models (HOT, HEF, HET, see text for explanations). (a) horizontal displacements; (b) vertical displacements and (c) EDM and GPS elongations.

eastern flank of Mt. Etna. These factors have second-order effects on the deformation due to a pressurized source. We also tried to modify the boundary conditions running a FE model in which the western flank of Mt. Etna is buttressed by the surrounding mountain chain (by imposing vanishing displacements at the W end of the volcanic edifice). However, also this model failed to reproduce any significant asymmetry in the deformation field.

It appears then that topography and heterogeneities provide only minor perturbations to the deformation field produced by a pressurized source under elastic conditions. However, we are comparing different models only in correspondence to GPS stations, so it is quite difficult to appreciate not only small differences, but also the whole deformation pattern. A more detailed comparison between the DAVIS and the FE models is shown in Fig. 11, where the normalized vertical displacement is contoured in the summit area of Mt. Etna. Topography and heterogeneous structure affect the vertical deformation in two distinct ways. With respect to the model DAVIS, in HOT the two lobes corresponding to maximum values are more asymmetric and moved away from the summit along the SW–NE direction. This effect may be linked to the huge depression of the Valle del Bove, which is one of the most prominent features of Mt. Etna topography. Another difference in model HOT is that the vertical deformation is spread over a broader area (the light green area in HOT is wider). The opposite effect is caused by the elastic heterogeneities in model HEF, where the vertical deformation is focused in a smaller area. Also the pattern is smoother, being characterized by a single area of maximum elongated in the SW–NE direction. The HET model combines both effects described before. With respect to DAVIS, it shows a more restricted deformation with the two maxima slightly asymmetrically distorted. Therefore, specifically for the summit area, the superposition of topography and heterogeneities partially compensate each other so that and the final results of the heterogeneous case resemble the flat homogeneous case.

5 DISCUSSION AND CONCLUSIONS

In this paper, we used ellipsoid and spheroid source models, arbitrarily oriented in space, to invert a redundant data set of significant horizontal and vertical displacements observed in Mt. Etna from 1993 to 1997. Our results, based on the analytical models, suggest that the source is unequivocally vertically elongated and probably has modest dimensions ($\sim$3 km^3). The observed geodetic data show a strong signature of the source shape because the ratio between horizontal and vertical displacements is high. However, we emphasize that robust source inference can be made only by considering the full 3-D pattern of the observed deformation. Recent studies, carried out on ground deformation data observed with different techniques, have tried to constrain pressure sources by simple models in a homogeneous elastic medium (Lundgren *et al.* 2003; Obrizzo *et al.* 2004). Lundgren *et al.* (2003) have used data from the SAR interferometry recorded during the first 2 yr of the inflation (1993–1995). These data consist of the displacement component along the radar line of sight, which is near vertical, so that they are poorly sensitive to the horizontal deformation. Inversions based on these data suggest a large body (volume about 25 km^3) that is incompatible with the information from seismic tomography (e.g. no evidence of magma chamber with these dimensions is found by Chiarabba *et al.* 2000). Also the main axis, elongated horizontally, seems to hardly reconcile with the horizontal and vertical data measured by terrestrial and spatial geodesy. Obrizzo *et al.* (2004) modelled only one displacement component, that is, the vertical changes from levelling measurements, by using a simple Mogi (1958) source. This source, even though successful in reproducing the vertical components, would not be able to take into account the 3-D displacement field (horizontal and vertical changes) measured by EDM and GPS networks.

Our findings suggest that the results from source inversions should always be interpreted by trying to integrate all the available information, possibly comparing with inferences drawn from other disciplines (such as seismology, geochemistry, gravimetry) and keeping in mind the evolution of the different phases of volcanic activity. Seismic tomography investigations (Chiarabba *et al.* 2000; Laigle *et al.* 2000; Patanè *et al.* 2002) have not shown the presence of a large low-seismic v_p anomalous region beneath the volcano summit which could be interpreted as a magma chamber. On the other hand, the main common feature of all the tomographic investigations on Mt. Etna is a high v_p body embedded in the pre-Etnean sediments from 3 to 9 km depth and extending laterally for 8–10 km beneath the central and eastern part of the volcano. This body would represent a plexus of solidified intrusions. During this recharging phase, all the seismicity was located around the boundaries of this body, being

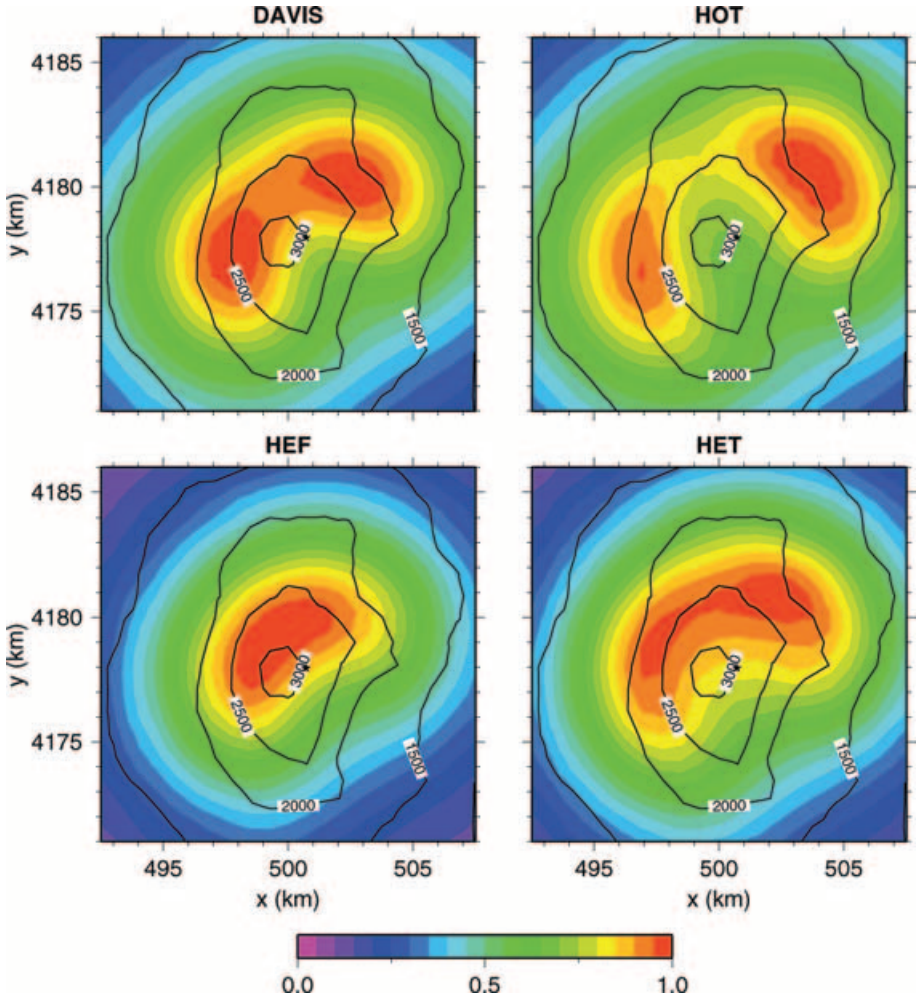

Figure 11. Normalized vertical displacement in the summit area of Mt. Etna for the homogeneous and heterogeneous models with or without topography (see text for a description). The black lines correspond to the topography contoured from 1500 to 3000 m every 500 m. DAVIS, HOT, HEF and HET are: homogeneous flat, homogeneous with topography, heterogeneous flat and heterogeneous with topography models, respectively.

almost absent inside (Patanè *et al.* 2003). The authors argued that the magma probably rose along the western margin of this body, located under the crater area, and the increasing pressure against the hosting rocks caused seismic activity. The uprising along this path may have stopped and allowed the magma to stagnate at different depths, in agreement with the buoyancy level due to its density between 15 km and the sea level (Corsaro & Pompilio 2004). Furthermore, also a recent attenuation tomography study (De Gori *et al.* 2005) envisages a highly attenuative body, extending vertically and characterized by similar dimensions, between 5 km below and 1 km above sea level. Our finding of a small vertical elongated source beneath the craters is in agreement with these interpretations of the post-1997 activity.

The inferred source parameters, however, are not able to predict the enhanced horizontal displacements recorded in the lower SE sector of Mt. Etna. The inclusion of these data in the inversion procedure may have introduced a significant bias in the retrieved source parameters, as discussed previously. However, this may have affected mostly the position of the source but not its vertically elongated shape, which we found to be a robust feature of the inversions.

FE numerical models, based on the analytical inversion results, have been carried out with the aim of evaluating the effects caused by the real topography and elastic stratification of Mt. Etna. Our numerical models were motivated by the need to overcome the limitations of the analytical approach in order to mitigate the residuals obtained in the SE sector. While the representation of the topography is straightforward, the implementation of internal elastic heterogeneities computed from seismic tomography requires a series of assumptions. We have already seen that the elastic rheology is an overly constrained approximation for volcanic environments, where the medium may be viscoelastic (due to the high temperatures) or elastoplastic (due to the low strength and low confining pressure of shallow volcanic rocks). The elastic rheology is inappropriate because, if the source volume is below the resolving power of seismic tomography, we need an exceedingly high overpressure to fit the observed displacements. It must be kept in mind that the strength of the deformation source is given by $\Delta PV/\mu$. In order to reproduce large deformations with reasonable overpressure values, most studies assume an effective rigidity much lower than the seismically determined value: this is another way of saying that the medium is not perfectly elastic. For instance, the simplest constitutive law providing a short-term rigidity higher than the long-term rigidity is the standard linear solid (SLS) rheology, which however requires specification of three parameters. Among these parameters the viscosity is strongly temperature dependent so that we would also need a rather detailed thermal structure of the volcano, which is unavailable at present. Trasatti *et al.* (2003) also showed that rheological

heterogeneities may be much more important than elastic heterogeneities in the long-term deformation. In any case, we may be confident that the inelastic properties concentrate near the source, where higher temperatures and higher deviatoric stresses are present. The effective volume of the source then would be greater than the reservoir, as suggested by Dragoni & Magnanensi (1989) and discussed by Newmann *et al.* (2001). However, in the FE models we preferred to use an effective overpressure $\Delta P'$, even though it is too high to be plausible within the magma, still maintaining the elastic rheology assumption and a low value for the source volume. In this way we have characterized the heterogeneities below Etna with their seismic rigidities, which are more realistic but notably greater than the average effective rigidity usually employed in homogeneous half-space models.

Our numerical computations clearly point out that heterogeneous model predictions can be significantly different from the simple homogeneous, flat elastic cases. Such perturbations are, however, more evident in presence of accentuated topography, for example, in the summit area, and in presence of severe heterogeneity, while further away from the summit they are more similar to the simplest cases. We conclude that these heterogeneities scarcely impact a source inference based on a coarse sampling of the volcano, such as the GPS and EDM networks data in our case, while they could be important to interpret data with a better coverage of the volcano, such as SAR images. However, the heterogeneous models could be needed for detailed modelling of the deformation in the summit area of Mt. Etna, where high sensitivity geodetic instruments are installed. Since the effects of the heterogeneities are mainly confined to the volcano summit, they cannot play a significant role in amplifying the deformation in the SE sector, which is probably due to other mechanisms than the inflation of an internal source.

Future research should be focused on extracting viscoelastic or elastoplastic parameters pertinent to Mt. Etna, modelling the sliding movement of the SE sector and taking into account the deformation of rifts and faults, which may decouple the SE sector from the rest of the volcanic edifice.

ACKNOWLEDGMENTS

We are indebted to the Deformation Group of the Istituto Nazionale di Geofisica e Vulcanologia Sezione di Catania for having collected the GPS and EDM measurements. In particular, we thank G. Puglisi and A. Bonforte who planned the field measurement campaigns and elaborated the data. We also acknowledge P. De Gori and D. Patané for providing seismic tomography data and N. Feuillet for fruitful discussions. This work was supported by grants from the INGV-DPC 2004–2006 project.

REFERENCES

Alparone, S., Andronico, D., Lodato, L. & Sgroi, T., 2003. Relationship between tremor and volcanic activity during the Southeast Crater eruption on Mount Etna in early 2000, *J. geophys. Res.,* **108**(B5) 2241, doi:10.1029/2002JB001866.

Behncke, B. & Neri, M., 2003. The July-August 2001 eruption of Mt. Etna (Sicily)., *Bull. Volcanol.,* **65**(7), 461–476.

Bonaccorso, A., 1996. Dynamic inversion of ground deformation data for modelling volcanic sources (Etna 1991–93), *Geophys. Res. Lett.,* **23**(5), 451–454.

Bonaccorso, A. & Davis, P.M., 2004. Modeling of ground deformation associated with recent lateral eruptions: Mechanics of magma ascent and intermediate storage at Mt. Etna, in *Mount Etna Volcano Laboratory*, Vol. 143, p. 384, eds Bonaccorso, A., Calvari, S., Coltelli, M., Negro, C.D. & Falsaperla, S., American Geophysical Union Monography Series.

Bonaccorso, A. & Patanè, D., 2001. Shear response to an intrusive episode at Mt. Etna volcano (January 1998) inferred through seismic and tilt data, *Tectonophysics,* **334,** 61–75.

Bonafede, M. & Rivalta, E., 1999. On tensile cracks close to and across the interface between two welded elastic half-spaces, *Geophys. J. Int.,* **138,** 410–434.

Bonforte, A. & Puglisi, G., 2003. Magma uprising and flank dynamics on Mt. Etna volcano, studied using GPS data (1994–1995), *J. geophys. Res.,* **108,** 2153–2162.

Borgia, A., Ferrari, L. & Pasquarè, G., 1992. Importance of gravitational spreading in the tectonic and volcanic evolution of Mt. Etna, *Nature,* **357,** 231–234.

Budetta, G., Carbone, D. & Greco, F., 1999. Subsurface mass redistributions at Mount Etna (Italy) during the 1995–1996 explosive activity detected by microgravity studies, *Geophys. J. Int.,* **138,** 77–88.

Carbone, D., Budetta, G. & Greco, F., 2003. Bulk processes prior to the 2001 Mount Etna eruption, highlighted through microgravity studies, *J. geophys. Res.,* **108**(B12) 2556, doi:10.1029/2003JB002542.

Chiarabba, C., Amato, A., Boschi, E. & Barberi, F., 2000. Recent seismicity and tomographic modeling of the Mount Etna plumbing system, *J. geophys. Res.,* **105**(B5), 10 923–10 938.

Chiarabba, C., De Gori, P. & Patanè, D., 2004. The Mt. Etna plumbing system: The contribution of seismic tomography, in *Mount Etna Volcano Laboratory*, Vol. 143, p. 384, eds Bonaccorso, A., Calvari, S., Coltelli, M., Negro, C.D. & Falsaperla, S., American Geophysical Union Monography Series.

Corsaro, R. & Pompilio, M., 2004. Buoyancy-controlled eruption at Mt. Etna, *Terranova,* **16,** 16–22.

Davis, P.M., 1986. Surface deformation due to inflation of an arbitrarily oriented triaxial ellipsoidal cavity in an elastic half-space, with reference to Kilauea volcano, Hawaii, *J. geophys. Res.,* **91,** 7429–7438.

Davis, P.M., Hastie, L.M. & Stacey, F.D., 1974. Stresses within an active volcano — with particular reference to Kilauea, *Tectonophysics,* **22,** 355–362.

De Gori, P., Chiarabba, C. & Patanè, D., 2005. Qp structure of Mt. Etna: constraints for the physics of the plumbing system, *J. geophys. Res.*, **112,** B05303, doi:10.1029/2003JB002875.

Dragoni, M. & Magnanensi, C., 1989. Displacement and stress produced by a pressurized spherical magma chamber surrounded by a viscoelastic shell, *Phys. Earth planet. Int.,* **56,** 316–328.

Froger, J.L., Merle, O. & Briole, P., 2001. Active spreading and regional extension at Mount Etna imaged by SAR interferometry, *Earth planet. Sci. Lett.,* **187,** 245–258.

Jaeger, J.C., 1969. *Elasticity, Fracture and Flow*, Chapman and Hall, London.

La Delfa, S., Patanè, G., Clocchiatti, R., Joron, J.L. & Tanguy, J.C., 2001. Activity preceding the February 1999 fissure eruption: inferred mechanism from seismological and geochemical data, *J. Volc. Geotherm. Res.,* **105,** 121–139.

Laigle, M., Hirn, A., Sapin, M., Lepine, J.C., Diaz, J., Gallart, J. & Nicolich, R., 2000. Mt. Etna dense array local earthquake P and S tomography and implications for volcanic plumbing, *J. geophys. Res.,* **105,** 21 633 –21 646.

Lanari, R., Lundgren, P. & Sansosti, E., 1998. Dynamic deformation of Etna volcano observed by satellite radar interferometry, *Geophys. Res. Lett.,* **25**(10), 1541–1544.

Lo Giudice, E. & Rasà, R., 1996. The role of the NNW structural trend in the recent geodynamic evolution of North-Eastern Sicily and its volcanic implications in the Etnean area, *J. Geodyn.,* **5,** 309–330.

Lundgren, P., Berardino, P., Coltelli, M., Fornaro, G., Lanari, R., Puglisi, G., Sansosti, E. & Tesauro, M., 2003. Coupled magma chamber inflation and sector collapse slip observed with synthetic aperture radar interferometry on Mt. Etna volcano, *J. geophys. Res.,* **108**(B5) 2247, doi:10.1029/2001JB000657.

Marquardt, D.W., 1963. An algorithm for least estimation of non-linear parameters, *J. Soc. Ind. Appl. Math.,* **11,** 431–441.

Massonnet, D., Briole, P. & Arnaud, A., 1995. Deflation of Mt. Etna monitored by spaceborne radar interferometry, *Nature,* **375,** 567–570.

Mogi, K., 1958. Relation between the eruptions of various volcanoes and deformations of the ground surfaces around them, *Bull. Earth Res. Inst.,* **36,** 99–134.

Mosegaard, K. & Tarantola, A., 1995. Monte Carlo sampling of solutions to inverse problems, *J. geophys. Res.,* **100**(B7), 12 431–12 447.

Neri, M., Acocella, V. & Behncke, B., 2004. The role of the Pernicana Fault system in the spreading of Mt. Etna (Italy) during the 2002–2003 eruption, *Bull. Volcanol.,* **66,** 417–430.

Newmann, A.V., Dixon, T., Ofoegbu, G. & Dixon, J., 2001. Geodetic data constraints on recent activity at Long Valley Caldera, California: evidence for viscoelastic rheology, *J. Volc. Geotherm. Res.,* **105,** 183–206.

Obrizzo, F., Pingue, F., Troise, C. & De Natale, G., 2004. Bayesian inversion of 1994–98 vertical displacements at Mt. Etna; evidence for magma intrusion, *Geophys. J. Int.,* **157**(2), 935–946.

Patanè, D., Chiarabba, C., Cocina, O., De Gori, P., Moretti, M. & Boschi, E., 2002. Tomographic images and 3D earthquakes locations of the seismic swarm preceding the 2001 Mt. Etna eruption: evidence for a dike intrusion, *Geophys. Res. Lett.,* **29**(10) 1497, doi:10.1029/2001GL014391.

Patanè, D., De Gori, P., Chiarabba, C. & Bonaccorso, A., 2003. Magma ascent and the pressurization of Mount Etna's volcanic system, *Science,* **299**(5615), 2061–2063.

Press, W.H., Teukolsky, S.A., Vetterling, W.T. & Flannery, B.P., 1997. *Numerical Recipes in Fortran*, Cambridge University Press, New York.

Puglisi, G., Bonforte, A. & Maugeri, S.R., 2001. Ground deformation patterns on Mt. Etna, 1992 to 1994, inferred from GPS data, *Bull. Volcanology,* **62,** 371–384.

Rust, D. & Neri, M., 1996. The boundaries of large-scale collapse on the flanks of Mt. Etna, Sicily, in *Volcano instability on the earth and other planets*, Vol. 110, pp. 193–198, eds, McGuire, W. J., Jones A. P. & Neuberg J., Geol. Soc. Lond. Spec. Pub.

Trasatti, E., Giunchi, C. & Bonafede, M., 2003. Effects of topography and rheological layering on ground deformation in volcanic regions, *J. Volc. Geotherm. Res.,* **122,** 89–110.

Yang, X., Davis, P.M. & Dieterich, J., 1988. Deformation from inflation of a dipping, finite, prolate ellipsoid in an elastic half-space, *J. geophys. Res.,* **93,** 4249–4257.